Synthesis of Dense Poly(acrylic acid) Brushes and Their Interaction with Amine-Functional Silsesquioxane Nanoparticles

Markus Retsch,[†] Andreas Walther,[†] Katja Loos,[‡] and Axel H. E. Müller*,[†]

Makromolekulare Chemie II and Bayreuther Zentrum für Kolloide and Grenzflächen, Universität Bayreuth, 95440 Bayreuth, Germany, and Department of Polymer Chemistry, Zernike Institute for Advanced Materials, University of Groningen, 9747AG Groningen, The Netherlands

Received March 28, 2008. Revised Manuscript Received May 18, 2008

Poly(acrylic acid) polyelectrolyte brushes were synthesized by surface-initiated atom transfer radical polymerization (SI-ATRP) of *tert*-butyl acrylate on planar gold surfaces and subsequent hydrolysis. Three types of monolayers with different numbers of thiol binding sites per initiating unit were used. The binding strength to the gold surface turned out to be of crucial importance for the formation of uniform brush layers after acidic hydrolysis. The monolayers and polymer brushes were characterized by ellipsometry, infrared spectroscopy, water contact angle measurements, atomic force microscopy, and X-ray photoelectron spectroscopy. Their interaction with [(diglycidylamino)propyl]silsesquioxane nanoparticles at various pH values was studied by surface plasmon resonance.

Introduction

Over the past decade the development of nanotechnology has become increasingly important. A vast range of materials on the nanometer scale have been developed either by downsizing existing technologies ("top down") or by building up structures from single molecules ("bottom up"). The surface of objects on the nanometer scale plays a major role since their properties are governed by their huge interface. Controlling the surface properties of any material in the nanometer range is the linchpin to adjust its properties and its interaction potential. Alongside advances in polymer synthesis, the field of polymer/hybrid complexes has evolved. The combination of the physical properties of polymers with those of inorganic or biological moieties often yields highly interesting hybrid materials with novel and superior properties. They are therefore promising candidates for future high-tech materials and also biotechnological applications. Nevertheless, to fully control polymer−hybrid complexes, more research needs to be done to elucidate the fundamental interaction parameters.

Polymer brushes (defined as a layer consisting of polymer chains tethered to a surface) offer excellent possibilities to tailor surface properties. Two methods are commonly used to obtain polymer brushes, "grafting to" and "grafting from". The former attaches prebuilt polymers by reactive end or side groups to functional surfaces, yielding thin layers of low grafting density. This derives from the steric hindrance between attached and free polymer during the deposition step.[1] Using the grafting from method, the polymer brush grows from a surface covered with an initiator species, and this is the superior alternative as the functionality, density, and thickness of the polymer brushes can be controlled with almost molecular precision. During the past decade extensive work has been performed on the implementation of common polymerization techniques to surface-initiated polymerization (SIP). Anionic,[2,3] cationic,[4] and ring-opening metathesis (ROMP)[5] polymerizations have been adapted to SIP. Free radical polymerization[6] has been established, and also controlled radical polymerizations can be carried out: nitroxide-mediated polymerization (NMP) was introduced by Hussemann et al.[7] In reversible addition fragmentation chain transfer (RAFT) polymerization the chain transfer agent was immobilized by either its Z-group or its R-group to the surface as reported by Li and Benicewicz.[8] In surface-initiated atom transfer radical polymerization (SI-ATRP), the initiator (in most cases an α-bromoester derivative) is attached to the solid surface and polymerization can be conducted with or without sacrificial initiator in the solution as demonstrated by Ejaz et al.[9] and von Werne et al.[10] The use of a sacrificial initiator opens the way to estimate the molecular weight of the grafted polymer. As long as the molecular weight evolution of the free polymer and the thickness growth of the polymer layer exhibit the same kinetics, one can assume that the molecular weights of the two species are similar.[11] A direct comparison of grafted and free polymer can be undertaken when polymerization is done from spherical particles and the chains are cleaved from the particles.[10,12] Those studies showed that the molecular weights of the immobilized and the free polymer are roughly the same. Knowledge of the number-average molecular weight, M_n, of the grafted polymer is mandatory to determine the grafting density, σ, of the polymer.[13]

The use of polyelectrolytes (PELs) instead of neutral polymers results in a class of materials with highly interesting behavior due to their high electrostatic potential within the layer: so-

* To whom correspondence should be addressed. E-mail: axel.mueller@uni-bayreuth.de.

[†] Universität Bayreuth.

[‡] University of Groningen.

(1) Kopf, A.; Baschnagel, J.; Wittmer, J.; Binder, K. *Macromolecules* **1996**, *29*, 1433.

(2) Advincula, R.; Zhou, Q.; Park, M.; Wang, S.; Mays, J.; Sakellariou, G.; Pispas, S.; Hadjichristidis, N. *Langmuir* **2002**, *18*, 8672.

(3) Jordan, R.; Ulman, A.; Kang, J. F.; Rafailovich, M. H.; Sokolov, J. *J. Am. Chem. Soc.* **1999**, *121*, 1016.

(4) Jordan, R.; Ulman, A. *J. Am. Chem. Soc.* **1998**, *120*, 243.

(5) Weck, M.; Jackiw, J. J.; Rossi, R. R.; Weiss, P. S.; Grubbs, R. H. *J. Am. Chem. Soc.* **1999**, *121*, 4088.

(6) Prucker, O.; Rühe, J. *Macromolecules* **1998**, *31*, 592.

(7) Hussemann, M.; Malmström, E. E.; McNamara, M.; Mate, M.; Mecerreyes, D.; Benoit, D. G.; Hedrick, J. L.; Mansky, P.; Huang, E.; Russell, T. P.; Hawker, C. J. *Macromolecules* **1999**, *32*, 1424.

(8) Li, C. Z.; Benicewicz, B. C. *Macromolecules* **2005**, *38*, 5929.

(9) Ejaz, M.; Yamamoto, S.; Ohno, K.; Tsujii, Y.; Fukuda, T. *Macromolecules* **1998**, *31*, 5934.

(10) von Werne, T.; Patten, T. E. *J. Am. Chem. Soc.* **2001**, *123*, 7497.

(11) Ramakrishnan, A.; Dhamodharan, R.; Rühe, J. *J. Polym. Sci., Part A: Polym. Chem.* **2006**, *44*, 1758.

(12) Ohno, K.; Koh, K.; Tsujii, Y.; Fukuda, T. *Macromolecules* **2002**, *35*, 8989.

(13) Mori, H.; Böker, A.; Krausch, G.; Müller, A. H. E. *Macromolecules* **2001**, *34*, 6871.

10.1021/la8009767 CCC: $40.75
Published on Web 07/29/2008

Scheme 1. ATRP Initiators and Nanoparticles Used in This Study

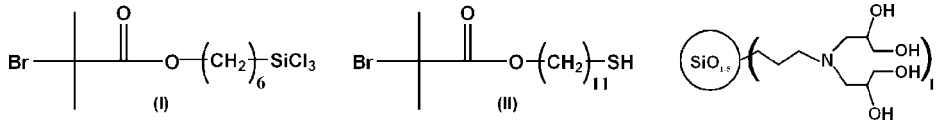

called polyelectrolyte brushes.[14] Depending on the type of monomer, the properties of the layer can be switched by external stimuli such as the pH, ionic strength, or temperature. A comprehensive theory about the behavior of polyelectrolyte brushes on planar and spherical surfaces was established during the 1990s.[15–21] Experimental confirmation of the predicted data, however, has only been possible for the past few years.

The ability of polyelectrolytes to switch their properties upon external stimuli and thereby change their mutual interaction and their interaction with other particles attracts interest to use them for polymer/hybrid complexes. Mori et al. reported on the pH-dependent interaction of free poly(acrylic acid) (PAA) and silsesquioxane nanoparticles.[22] The question we want to elucidate in this paper is at which pH the interaction between PAA brushes and silsesquioxane nanoparticles is highest.

Surface plasmon resonance (SPR) was chosen as a method to determine the interaction in real time. SPR is beneficial due to its ease of use, its sensitivity, and its ability to allow kinetic measurements.[23] A thin metal layer (in most cases gold) is prerequisite to allow SPR measurements. Therefore, controlled layers of PAA had to be grafted from gold-coated glass substrates. To reach a maximum of control and uniformity of the grafted polymer layer, atom transfer radical polymerization (ATRP) was chosen.

Experimental Section

Reagents. All solvents were p.a. grade and used without further purification if not specified otherwise. Toluene was distilled over CaH_2 and Na/K alloy and was stored under argon. *tert*-Butyl acrylate (tBA; 98%, Aldrich) was passed over a basic alumina column to remove the inhibitor and was stored under N_2 in the fridge.

11-Mercaptoundecyl 2-bromoisobutyrate[24] (**II**) and 5-(trichlorosilyl)pentyl 2-bromoisobutyrate[7] (**I**) were synthesized according to the literature.

Amine-functional silsesquioxane nanoparticles were synthesized according to the literature.[25] They feature a diameter of ~3 nm and a molecular weight of ~3760 g/mol and carry about 14 diglycidylamino functions per core; a sketch is given in Scheme 1.

Ethyl 2-bromoisobutyrate (EBIB; 98% Aldrich) and *N*,*N*,*N*′,*N*″,*N*″-pentamethyldiethylenetriamine (PMDETA; 99%, Aldrich) were distilled at high vacuum and stored under argon.

3-Mercapto-1-propanol (3-MPol; 95%), copper(I) bromide (CuBr; 99.9%), methanesulfonic acid (99%), (3-mercaptopropyl)trimethoxysilane (3-MPTMS; 95%), and triethylamine (99%) (Aldrich) were used as received.

Surface Preparation. The substrates (glass slides (Präzisionsglas & Optik GmbH) and silicon wafers, respectively) were cleaned by two cycles of sonication with 2% Hellmanex (Hellma GmbH) for 15 min and extensive rinsing with Milli-Q water. Finally, the substrates were rinsed with ethanol and dried in a stream of nitrogen. The deposition of the metal layer was conducted in a BALZERS BA 510 sputtering machine. The pressure during deposition was 2×10^{-5} mbar; the source was an electron beam gun. The deposited layer thickness was controlled using an oscillating quartz crystal. The deposition rate of chromium was set to 2 Å/s and the rate of gold to 10 Å/s. Layer thicknesses were adjusted to 2 nm of Cr and 50 nm of Au. The gold surfaces were prepared freshly before monolayer formation to prevent unnecessary contamination of the surface.

Monolayer Formation. Three different kinds of monolayers were synthesized and are denoted as monopod (**a**), tripod (**b**), and cross-linked (**c**) self-assembled monolayers (SAMs).

*Monopod Monolayer (**a**).* The substrates were deposited in a weighing glass with a solution of 13 mg of **II** in 20 mL of EtOH (HPLC grade, ~2 mM). The weighing glass was set under argon, and formation of the SAM was allowed for five days. Afterward the substrates were extensively washed with EtOH (p.a.) and dried in a stream of N_2.

*Tripod Monolayer (**b**).* The substrates were immersed in a solution of 9.2 mg of 3-MPol in 50 mL of EtOH (HPLC grade). SAM formation was allowed for eight days. Afterward the dried substrates were put in a dry screw-thread flask and set under argon. After they were covered with a layer of 5 mL of dry toluene, 0.5 mL of **I** was added. Finally, 0.5 mL of triethylamine was added dropwise. The flask was kept under argon and was gently shaken for 1 h. Finally, the substrates were washed with copious amounts of MeOH and dichloromethane (DCM). The substrates were stored in DCM and blown dry with N_2 prior to use.[7]

*Cross-Linked SAM (**c**).* The substrates were incubated in a solution of 21.1 mg of 3-MPTMS in 25 mL of dry MeOH (~4 mM). The SAM formation was allowed to proceed for 6.5 h. The sol−gel process among the immobilized trimethoxysilane groups was done by immersion of the substrates in a 0.1 M HCl solution for 4.5 h. After that the substrates were rinsed with Milli-Q water and dried with nitrogen.[26] The immobilization of the ATRP initiator was conducted in a glovebox. A 0.4 mL portion of the solution of **I** was dissolved in 6 mL of dry toluene and placed over the substrates in a weighing glass. Triethylamine (0.31 mL) was dispersed in 4 mL of dry toluene and was added slowly and evenly over the entire solution in the weighing dish. The reaction was allowed to proceed for 4 h. Finally, each substrate was immersed in 6 mL of DCM, rinsed twice with MeOH, and stored under DCM. Prior to use they were blown dry with N_2.[7]

Surface-Initiated Polymerization. The reaction mixture was typically weighed in a glovebox. A 27.3 mg (0.73 mmol) portion of PMDETA, 24.4733 g (0.19 mol) of tBA, and 70.2 mg (0.489 mmol) of Cu(I) were weighed into a 50 mL screw-thread bottle. After the Cu(I) was dissolved, 0.824 mg (7.62 mmol) of anisole and 15.6551 g (0.270 mol) of acetone were added. After the solution was stirred for another 5 min 47.7 mg (0.2448 mmol) of EBIB was added. The clear, light green solution was well stirred and finally dispersed in ca. 10 mL screw-thread round-bottom flasks, which

(14) Rühe, J.; Ballauff, M.; Biesalski, M.; Dziekok, P.; Gröhn, F.; Johannsmann, D.; Houbenov, N.; Hugenberg, N.; Konradi, R.; Minko, S.; Motornov, M.; Netz, R. R.; Schmidt, M.; Seidel, C.; Stamm, M.; Stephan, T.; Usov, D.; Zhang, H. *Adv. Polym. Sci.* **2004**, *165*, 79.
(15) Ross, R. S.; Pincus, P. *Macromolecules* **1992**, *25*, 2177.
(16) Lyatskaya, Y. V.; Leermakers, F. A. M.; Fleer, G. J.; Zhulina, E. B.; Birshtein, T. M. *Macromolecules* **1995**, *28*, 3562.
(17) Zhulina, E. B.; Birshtein, T. M.; Borisov, O. V. *Macromolecules* **1995**, *28*, 1491.
(18) Borisov, O. V.; Zhulina, E. B.; Birshtein, T. M. *Macromolecules* **1994**, *27*, 4795.
(19) Zhulina, E. B.; Borisov, O. V.; Brombacher, L. *Macromolecules* **1991**, *24*, 4679.
(20) Borisov, O. V.; Birshtein, T. M.; Zhulina, E. B. *J. Phys. II* **1991**, *1*, 521.
(21) Israels, R.; Leermakers, F. A. M.; Fleer, G. J.; Zhulina, E. B. *Macromolecules* **1994**, *27*, 3249.
(22) Mori, H.; Müller, A. H. E.; Klee, J. E. *J. Am. Chem. Soc.* **2003**, *125*, 3712.
(23) Knoll, W. *Annu. Rev. Phys. Chem.* **1998**, *49*, 569.
(24) Jones, D. M.; Brown, A. A.; Huck, W. T. S. *Langmuir* **2002**, *18*, 1265.
(25) Mori, H.; Lanzendörfer, M. G.; Müller, A. H. E.; Klee, J. E. *Macromolecules* **2004**, *37*, 5228.
(26) Kambhampati, D. K.; Jakob, T. A. M.; Robertson, J. W.; Cai, M.; Pemberton, J. E.; Knoll, W. *Langmuir* **2001**, *17*, 1169.

contained the initiator-immobilized surfaces. Approximately 3.5 mL of polymerization mixture was used for each substrate. The flasks were sealed with a rubber septum, which allowed samples to be taken throughout the polymerization.[27]

The polymerization was conducted at a temperature of 60 °C. Samples were repeatedly taken during the reaction to measure the conversion. The polymerization was stopped by addition of DCM and THF and exposure to air. The substrates were rinsed with copious amounts of THF (p.a.). To remove any adsorbed polymer on the grafted layer, the substrates were subjected to Soxhlet extraction in THF for at least 6 h.

The free polymer generated by the sacrificial initiator in the solution was passed through a silica gel column to remove the copper catalyst and was analyzed by GPC.

Hydrolysis of Poly(*tert*-butyl acrylate) (PtBA) Brushes. A 100 μL portion of methanesulfonic acid ($MeSO_3H$) was dissolved in 10 mL of DCM.[28] The PtBA-grafted substrates were immersed in the solution for various amounts of time. The duration of the hydrolysis was subjected to kinetic analysis. Afterward the substrates were immediately rinsed with copious amounts of EtOH and dried in a stream of nitrogen.

Silsesquioxane Nanoparticle Solutions. For the SPR measurement 0.1, 1.0, and 10.0 mg/mL solutions of silsesquioxane nanoparticles were prepared and adjusted to a pH of 3.0, 3.6, 4.4, 5.3, 6.6, or 8.0 by titration of HCl or NaOH. Analogous buffer solutions of Milli-Q water were brought to the same pH.

Methods. Ellipsometric measurements were performed on a variable-angle spectroscopic rotating analyzer ellipsometer, Sentech 850, which is able to determine Ψ and Δ in a wavelength range between 350 and 850 nm. To determine the shape of the ellipse of the reflected light, the intensities were determined twice for 16 different analyzer positions. For all measurements, a retarder was used and the angle of incidence was varied from 40° to 70° in steps of 10°. The measured data were evaluated using the fit models provided with the software SpectraRay. A multilayer model was set up, which comprised the following layers: BK 7 (Schott) or silicon, 2 nm of chromium, gold, a Cauchy layer, and air. The fit parameters were the layer thickness (d) and index of refractivity (n_0 and n_1) of the Cauchy layer and the thickness (d_{Au}) of the underlying gold layer. Measurements were performed on three different spots on each sample. The average layer thickness and the standard deviations were determined.

Surface plasmon resonance (SPR) measurements were conducted on a BIACORE X setup. All measurements were conducted at 25 °C, and the flow rate was set to 40 μL/min. The substrates were handmade, and the procedure was outlined previously in this section. The substrates were allowed to equilibrate at a set pH, i.e., until a steady baseline was measured. The injection of the analyte was conducted by using the bubble technique. After the Eppendorf pipet was loaded with the desired amount for injection, 5 μL of air was sucked in, followed by another 5 μL of the injection solution. At the beginning of each run the response signal was shifted to zero response units for easier comparison among the various substrates and runs. In a few cases it was also necessary to shift the curves along the time scale, to match the various points of injections; those shifts amounted only to a few seconds.

Phase-modulated infrared reflection absorption spectroscopy (PM-IRRAS) spectra were recorded using a Bruker IFS66 v/s spectrometer with a PMIRRAS PM37 attachment equipped with an MCT detector (Bruker, Karlsruhe, Germany). Spectra were recorded and evaluated with the software OPUS, version 4.0. The angle of incidence of the infrared beam with respect to the surface normal was between 80° and 85°. Spectra were recorded with a spectral resolution of 4 cm^{-1} and collected using 1194 scans during 20 min.

Attenuated total reflectance Fourier transform infrared (ATR-FTIR) spectra were recorded on a Spectrum One FT-IR spectrometer from Perkin-Elmer equipped with a horizontal ATR unit. The measurements were performed by placing a drop of the specific liquid onto the ATR crystal. The spectra were recorded at a resolution of 4 cm^{-1}.

Scheme 2. Three Different Motifs of Initiator Immobilization

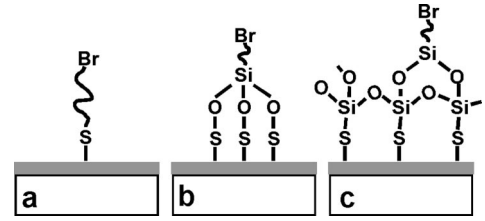

X-ray photoelectron spectroscopy (XPS) spectra were recorded using an SSX-100 (Surface Science Instruments) photoelectron spectrometer with a monochromatic Al Kα X-ray source ($h\nu$ = 1486.6 eV). The base pressure in the spectrometer was 1×10^{-9} Torr during the measurements.

Advancing water contact angle measurements were conducted with a contact angle system OCA setup from Dataphysics. The sessile drop configuration was used, and equal amounts of droplet volume were ensured by a micrometer screw. Snapshots were taken by a video camera. Shape analysis of the sessile drop was performed with the software SCA 20, and an Ellipse fitting was used in all cases. At least five drops were measured on each surface to give average contact angles and the standard deviation.

Atomic force microscopy (AFM) images were taken on a Digital Instruments Dimension 3100 operated in tapping mode. Offline data processing was done using the Nanoscope software V6.12r1. Scans of 3×3 μm were recorded.

Molecular weight distributions and averages were characterized by conventional gel permeation chromatography (GPC) using THF as the eluent with toluene as the internal standard, at a flow rate of 1.0 mL/min, at room temperature. Column set: 5 mm PSS SDV gel, 10^2, 10^3, 10^4, and 10^5 Å, 30 cm each. Injection volume: 20 μL of a 2 mg/mL solution. Detectors: Waters 410 differential refractometer and Waters photodiode array detector. Universal calibration based on narrow PS standards (PSS, Mainz) was used for the calibration of the column set. Prior to measurements the samples were filtered using 0.2 μm PTFE or Nylon filters. The measured molecular weights were linearly corrected to molecular weights that were obtained by MALDI ToF measurements.

Results and Discussion

Monolayer Formation. Three types of monolayers were synthesized, which varied in the number of binding sites to the gold surface per initiating moiety. These three different architectures are sketched in Scheme 2 and will be referred to as monopod SAM (**a**), tripod SAM (**b**), and cross-linked SAM (**c**).

The synthetic strategy varied from SAM **a** to SAMs **b** and **c**. In the former case, the initiator molecule (11-mercaptoundecyl 2-bromoisobutyrate[24] (**II**)) was first completely synthesized and then deposited on the gold surface. In the latter cases a monolayer of 3-MPol or cross-linked 3-MPTMS was immobilized on the substrate first. The initiator (5-(trichlorosilyl)pentyl 2-bromoisobutytrate[7] (**I**)) was then bound to the deposited moieties by condensation of the trichlorosilane entity with free hydroxyl groups. In the case of the 3-MPol monolayer this procedure will lead to three sulfur bonds per initiating site, as long as contamination with free hydroxyl groups (i.e., not bound to the gold layer) is prevented. This could result in some cross-linking among the trichlorosilane groups, which could increase the binding sites per α-bromo ester group. In the case of the cross-linked 3-MPTMS SAM the trichlorosilane will readily react with free hydroxyl groups, which were created by acidic hydrolysis. Due to the cross-linking of 3-MPTMS a very dense and manifoldly fixed

(27) Treat, N. D.; Ayres, N.; Boyes, S. G.; Brittain, W. J. *Macromolecules* **2006**, *39*, 26.

(28) Dai, J.; Bao, Z.; Sun, L.; Hong, S. U.; Baker, G. L.; Bruening, M. L. *Langmuir* **2006**, *22*, 4274.

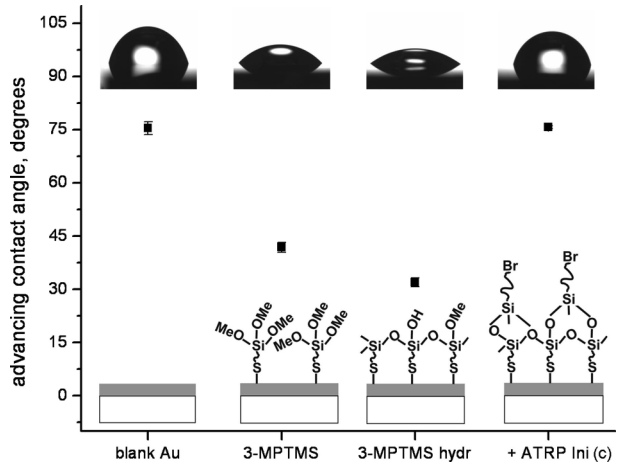

Figure 1. Water contact angle evolution during cross-linked monolayer formation. Snapshots of the sessile drop and sketches of the monolayer are also given in the graph.

layer is created. The successful formation of each SAM was monitored by PM-IRRAS, XPS, and water contact angle measurements.

The typical water contact angle evolution throughout the course of surface functionalization steps in the case of SAM **c** is shown in Figure 1. The corresponding graphs for the monopod and the tripod monolayers are presented in Figures S1 and S2 (Supporting Information).

The initial water contact angle for pure gold was repeatedly measured to be around 75°, which derives from adsorption of hydrophobic molecules from the atmosphere to the highly reactive gold surface. Upon deposition of 3-MPTMS the surface becomes more hydrophilic, which leads to a contact angle of about 42°. After hydrolysis the contact angle drops further to 32°, which originates from the cleavage of the methoxy groups. Deposition of the ATRP α-bromoester initiator **I** results in a more hydrophobic surface with a contact angle of 76°. Analogous results were obtained for all types of monolayers.

The successful formation of the desired monolayer was also confirmed by XPS measurements. A typical measurement for the course of monolayer formation as detected by XPS is shown in Figure 2 on the example of monolayer **c**. XPS spectra for the monopod and the tripod monolayers are available as Supporting Information, Figures S3 and S4, respectively.

The blank gold layer reveals the typical XPS peaks, which are indicated in Figure 2a.[29] Also some minor peaks in the carbon (284 eV) and oxygen (532 eV) regions were observed, which are assigned to impurities that adsorbed from the atmosphere to the freshly prepared gold layer. Upon deposition of 3-MPTMS the carbon and oxygen signals increase, and moreover, characteristic peaks for the silicon atom appear (Figure 2b). Pronounced peaks of the Si 2p signal were found after 3-MPTMS deposition and initiator immobilization. Only a slight increase in count rate was observed after hydrolysis of the sample, and no Si signal was present on the pure gold. Similar results were obtained for the other two types of monolayers.

PM-IRRAS measurements were carried out to characterize the monolayers more extensively. Figure 3 shows the spectrum of monolayer **a**. The corresponding measurements for the tripod and the cross-linked monolayers are given as Supporting Information, Figures S5 and S6.

The almost identical spectra of SAM **a** and bulk initiator **II** indicate successful immobilization of the initiator to the surface. Comparing the asymmetric (st as) and symmetric (st s) stretching modes of the methylene groups in our case (2927 and 2856 cm^{-1}, respectively) with the ones reported by Porter et al.[30] for pure alkanethiols with the structure $CH_3(CH_2)_{21}SH$, the measured values seem to be closer to the values found for the liquid (disordered) state (2924 and 2855 cm^{-1}, respectively) than to the values found for the crystalline (ordered) state (2918 and 2851 cm^{-1}, respectively).

The fact that the IR spectra of the bulk initiator and the SAM are equal also suggests that the monolayer is not in a perfect crystalline state, as the bulk sample is not in a crystalline form (drop of liquid on an ATR crystal).

In case of the tripod and cross-linked monolayers the successful deposition could be observed by the appearance of Si−O stretching modes in addition to the C═O signal.

The three characterization methods presented here strongly suggest the successful formation of the desired monolayer; however, they do not give an indication of the quality of the SAM. This issue can be addressed after the SIP by the evaluation of the achieved grafting density of the polymer.

Surface-Initiated Polymerization. The same polymerization conditions were applied to all three types of substrates. ATRP with a target degree of polymerization (DP) of 780 was carried out in acetone at a solid content of 60% and a temperature of 60 °C. The ratio among the initiator, copper, and ligand was 1:2:3. The layer thickness of the grafted brush was adjusted by quenching at different stages of conversion. The use of sacrificial initiator allowed measuring the molecular weight M_n of the free polymer in solution. The dependence of M_n on conversion is given in Figure 4 for all three polymerizations on the different substrates.

In all cases a linear relationship between conversion and molecular weight M_n was found. With increasing conversion the PDI decreased in most cases well below 1.1. Comparison of the theoretical and the experimental M_n resulted in initiator efficiencies from 75% to 100%. The first-order kinetic plot $\ln(M/M_0)$ versus time to the 2/3 power was also found to be linear.[31] Thus, the kinetic analysis of the tBA polymerization in the bulk solution indicates a well-controlled character of the polymerization and was independent of the type of monolayer that was present during polymerization.

The evolution of the layer thickness with time and conversion is shown in Figure 5. A linear relationship between the degree of polymerization and the achieved layer thickness is observed. Since this kinetic behavior is the same as for the M_n−conversion relationship of the free polymer, it can be assumed that the free and the grafted polymers possess similar molecular weights. Knowledge of M_n and the layer thickness d can be used to calculate the grafting density of the PtBA brushes on the gold surface using the equation $\sigma = 10^{-21} d\rho N_A/M_n$ (nm^{-2}), where ρ is the density of the polymer and N_A is Avogadro's constant.

Taking the bulk density of PtBA of 1.05 g/mL,[32] grafting densities $\sigma = 0.48 \pm 0.03$ nm^{-2}, 0.61 ± 0.05 nm^{-2}, and 0.51 ± 0.05 nm^{-2} are obtained for the polymers initiated by monolayers **a**, **b**, and **c**, respectively. The values presented are based on calculations for at least six samples per monolayer. The grafting densities indicate two things. First, the monolayer was assembled in a very homogeneous way on each sample, which is reflected

(29) Beamson, G.; Briggs, D. *High-Resolution XPS of Organic Polymers*; John Wiley & Sons: New York, 1992.

(30) Porter, M. D.; Bright, T. B.; Allara, D. L.; Chidseyi, C. E. D. *J. Am. Chem. Soc.* **1987**, *109*, 3559.

(31) Fischer, H. *Macromolecules* **1997**, *30*, 5666.

(32) Brandrup, J.; Immergut, E. H.; Grulke, E. A. *Polymer Handbook*, 4th ed.; John Wiley & Sons: New York, 1999.

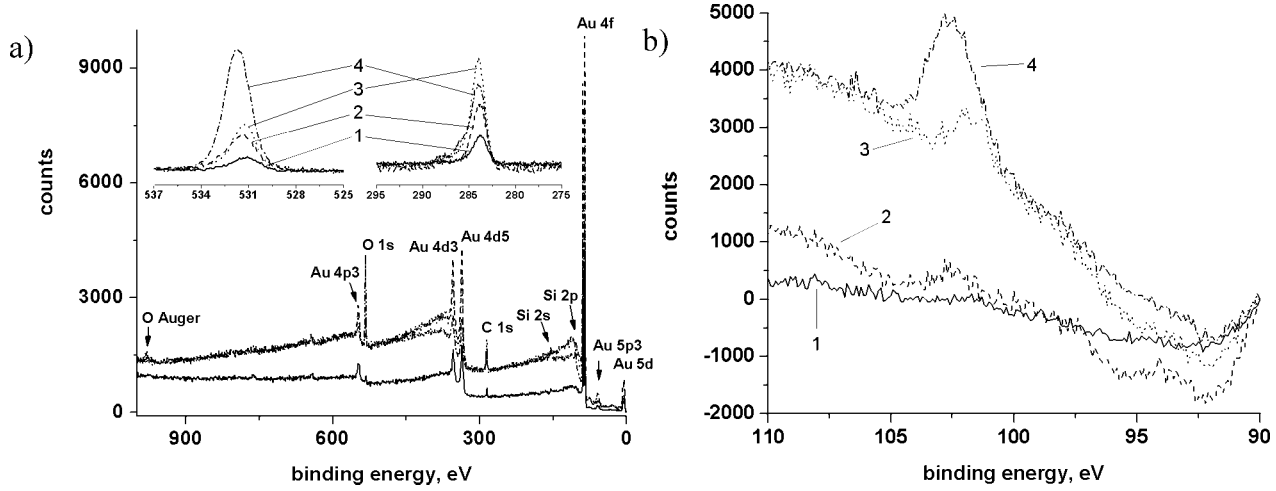

Figure 2. (a) XPS measurement of the monolayer formation steps for SAM **c**. Pure gold (solid line, 1), deposition of 3-MPTMS (dashed line, 2), hydrolysis of 3-MPTMS (dotted line, 3), and ATRP initiator immobilization (dashed-dotted line, 4) were overlaid. The two insets show enlargements of the O 1s and the C 1s peaks, respectively. (b) The enlargement of the Si 2p region shows the appearance of the Si atom after 3-MPTMS and initiator deposition.

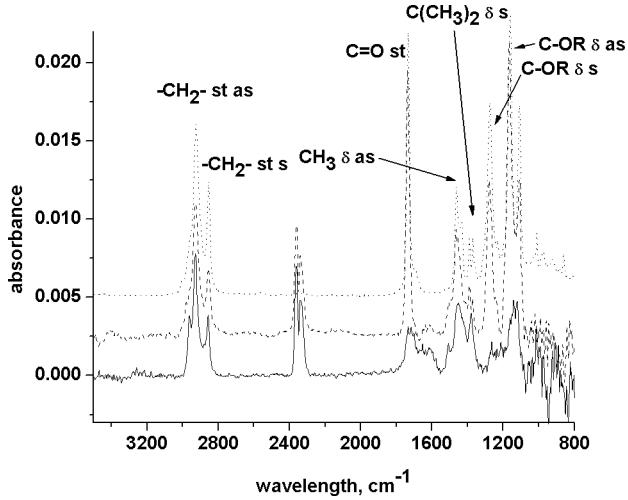

Figure 3. PM-IRRAS analysis of monopod monolayer formation: solid line, pure gold; dashed line, SAM **a**; dotted line: ATR-FTIR spectrum of a bulk droplet of the initiator.

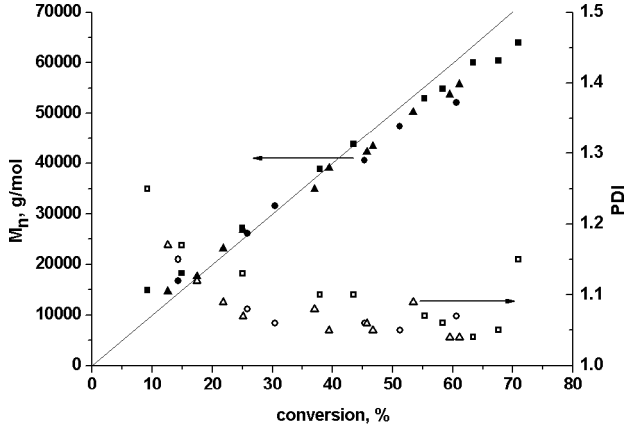

Figure 4. Molecular weight versus conversion plot for batch ATRP polymerization on (■) SAM **a**, (●) SAM **b**, and (▲) SAM **c**. Closed symbols represent M_n, and open symbol represent the corresponding polydispersity index. The straight line shows the theoretical M_n.

by the low standard deviation of below 10% for the grafting density in all cases. Second, the grafting densities differ only slightly from one monolayer to another. Therefore, it is reasonable to assume that the initiating sites on the surface are packed in a highly dense manner; the limiting factor for the grafting density of the polymer is then given by the bulkiness of the first monomers that add to the initiator and block the diffusion to other active centers in close vicinity.

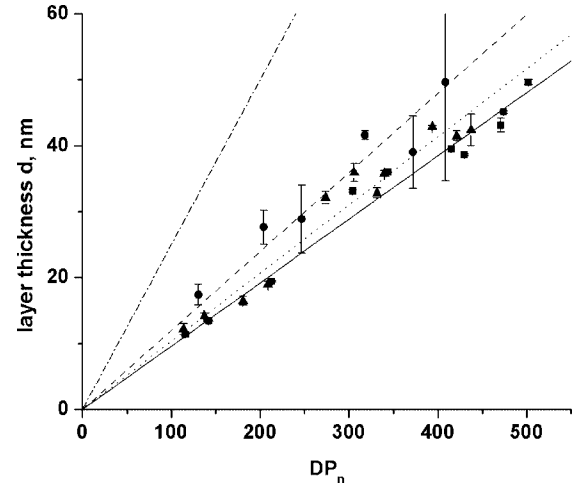

Figure 5. Dependence of the layer thickness on the degree of polymerization on substrates with three different monolayers as determined by ellipsometry: (■, solid line) SAM **a**, (●, dashed line) SAM **b**, and (▲, dotted line) SAM **c**. The straight lines are linear fits to the measured thicknesses; the dashed−dotted line shows the maximum layer thickness possible, when 0.25 nm per monomer unit is taken for calculation of the contour length.

Water contact angle measurements on the grafted PtBA layer repeatedly gave values between 84° and 89°. PM-IRRAS and XPS measurement results will be discussed in light of ester hydrolysis later on.

The smoothness of the brush layer was examined by AFM measurements on samples of various thicknesses for monopod substrate **a**, as shown in Figure 6. These measurements confirm that very homogeneous layers of PtBA were grafted onto the gold surface. The root-mean-square roughness (independent of the layer thickness) ranges from 0.7 to 1.3 nm and is therefore only slightly higher than the roughness of plain gold, which was measured to be 7 Å. The structure of the surface changes with increasing layer thickness. Initially the grains of the underlying

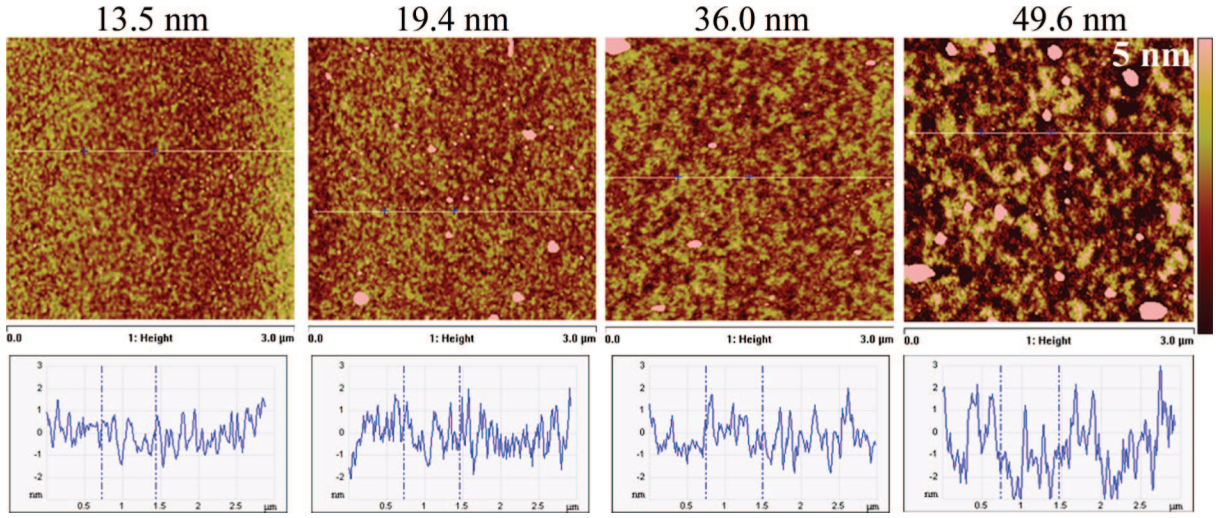

Figure 6. Topography and cross-sectional analysis of the grafted PtBA brushes at various layer thicknesses (3 × 3 μm height images).

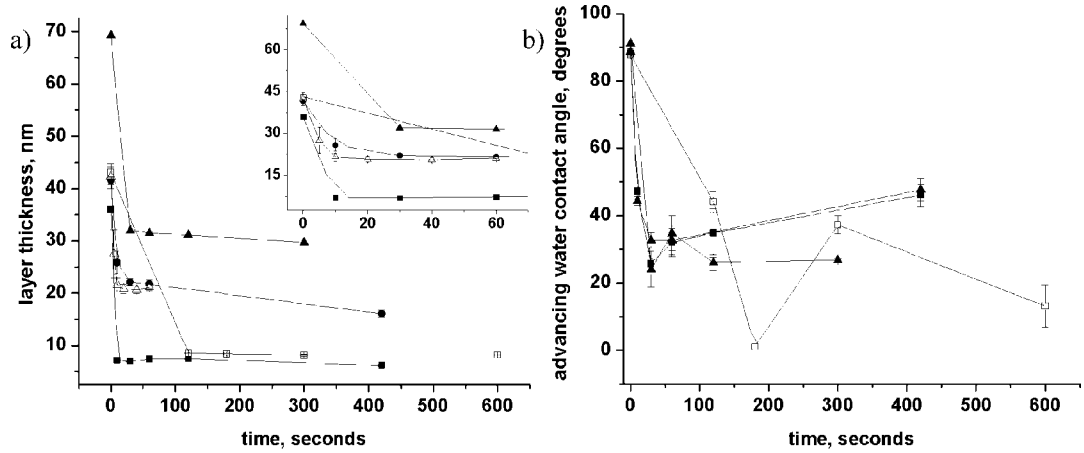

Figure 7. Kinetic analysis of the PtBA hydrolysis with methanesulfonic acid for different monolayers: (■) SAM **a**, (●) SAM **b**, and (▲) SAM **c**. Open and closed symbols refer to the same monolayer but different samples. (a) Decrease in layer thickness. The inset shows a zoom into the first 60 s of hydrolysis. (b) Evolution of the water contact angle. In both cases the solid lines are guides to the eye.

gold remain almost visible, giving a very subtle and fine structure. With increasing thickness this fine structure vanishes to be replaced by larger domains of a higher degree of variability in the surface structure.

So far it has been shown that both the monolayer and polymer brush were deposited in a very controlled and even way on the gold surface. The final step to obtain the desired PEL brush was to convert the PtBA into PAA by cleavage of the *tert*-butyl moiety.

Hydrolysis to PAA. Thermolytic cleavage[27] and various acidic pathways[28,33] to generate PAA were reported and also tried out in our group. It turned out that the binding strength of the initiating site to the gold surface is of crucial importance to retain control over the layer thickness, especially during acidic hydrolysis.

Acidic hydrolysis using methanesulfonic acid as described by Dai et al.[28] turned out to be most efficient and reproducible. Kinetic measurement of the hydrolysis was undertaken to evaluate the optimum time required. To do that, the substrates were simply taken out of the hydrolyzing solution and immediately rinsed with copious amounts of dichloromethane and ethanol. After measurement of the layer thickness by ellipsometry and water contact angle, the hydrolysis was continued. The result is shown in Figure 7.

The kinetic analysis proves a very rapid conversion of the PtBA into PAA. A quantitative conversion is achieved within only 60 s. This can be seen by the decrease in both the layer thickness and the water contact angle as a function of time. The water contact angle decreases when the hydrophobic *tert*-butyl moieties are cleaved away, leaving the very hydrophilic carboxylic acid that is easily wetted by water. Thus, the water contact angle decreases from about 90° to 20−40°. The large range derives from the fact that the water contact angle depends not only on the wettability of the surface functionalities, but also on the microstructure, which could change during hydrolysis. The layer thickness decreases as the bulky *tert*-butyl moiety is released. Due to that, voids within the polymer brush are created. These can be filled by the remaining polyelectrolyte by partial collapse of the backbone, which as a consequence lowers the layer thickness. As can be seen in Figure 7a the monolayer has a tremendous influence on the remaining layer thickness after hydrolysis. Usage of monolayers that bind with several sulfur atoms to the gold surface (**b** and **c**) result in stable polyelectrolyte layers after about 60 s. Monolayers **a**, however, result in very thin polyelectrolyte layers (thinner than 10 nm). To validate this result several samples of each type of monolayer were hydrolyzed

(33) Kurosawa, S.; Aizawa, H.; Talib, Z. A.; Atthoff, B.; Hilborn, J. *Biosens. Bioelectron.* **2004**, *20*, 1165.

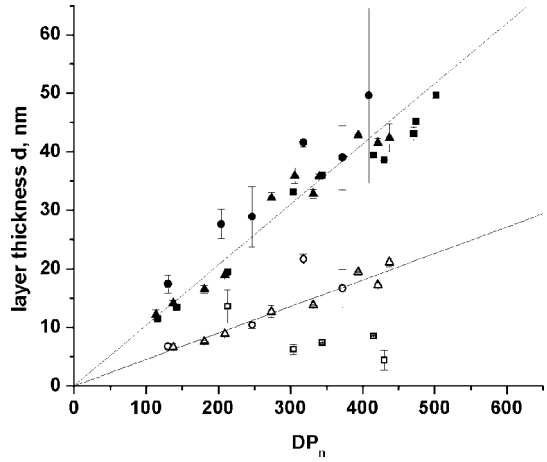

Figure 8. Decrease in layer thickness after hydrolysis of PtBA for 60 s in 1% methanesulfonic acid solution for each monolayer: (■) SAM **a**, (●) SAM **b**, and (▲) SAM **c**. The closed symbols show the layer thicknesses of the unhydrolyzed sample, and the open symbols show those of the hydrolyzed sample. The solid line is a linear fit to the triangular data points.

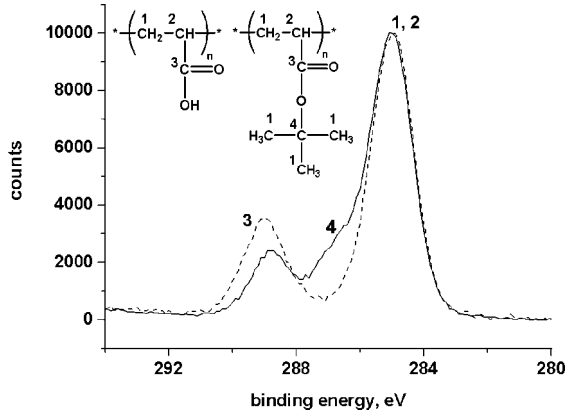

Figure 9. High-resolution XPS measurement of the C 1s signal before (solid line) and after (dashed line) hydrolysis with methanesulfonic acid.

under the optimum conditions: 60 s at room temperature. The decrease in layer thickness for all the types of substrates is shown in Figure 8.

Monolayers **b** and **c** are stable enough to sustain the acidic hydrolysis without cleavage of entire polymer chains. The decrease in layer thickness can be assigned to the gain in free volume by the release of the bulky *tert*-butyl group. Therefore, the decrease in layer thickness is almost the same for both types of monolayers and was calculated to be 58 ± 6% and 56 ± 3% for monolayers **b** and **c**, respectively. In the case of monolayer **a** entire polymer chains seem to be cleaved away. Since this process is kinetically driven and leaves more space for the remaining chains to collapse and change into a thermodynamically favored coiled conformation, the layer decreased to 28 ± 20% relative to the initial thickness. The large standard deviation indicates that this method is irreproducible.

To evaluate the feasibility of this hydrolysis method and to check the quantitative conversion, XPS (Figure 9) and PM-IRRAS (Figure 10) measurements were performed. The XPS measurement confirms the conversion of the *tert*-butyl moiety into carboxylic acid by the disappearance of the shoulder indicated by "4" in the graph. This shoulder can be assigned to the quaternary

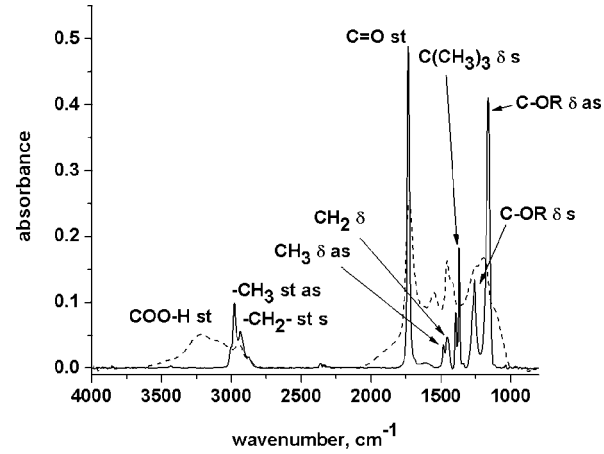

Figure 10. PM-IRRAS measurement before (solid line) and after (dashed line) hydrolysis.

C-atom of the *tert*-butyl group.[29] The PM-IRRAS measurement also affirms the quantitative conversion: the very characteristic double peak of the *tert*-butyl group at 1369 and 1394 cm^{-1} vanishes completely after hydrolysis. Furthermore, a broad shoulder from 3500 to 2800 cm^{-1} appears, which indicates the presence of carboxylic acid. AFM measurements proved that the PAA layer was still smooth and uniform; a roughness of 1.3 nm was measured.

Adsorption of Silsesquioxane Nanoparticles into the Poly(acrylic acid) Brushes. Due to their high stability, monolayers **c** were chosen to study the interaction between the silsesquioxane nanoparticles and the PAA brush. The pH was varied to determine where the interaction between the brush and nanoparticles was strongest. SPR experiments were conducted in a way that first the polyelectrolyte brush was allowed to reach equilibrium under the constant flow of buffer solution at a distinct pH. Then 80 μL of analyte solution containing the nanoparticles was injected; after the end of injection the flow was continued by the buffer. The interaction between the PAA brush and the nanoparticle can be determined from the increase in the SPR signal, here given in relative response units (ΔRU), which corresponds to changes in the layer thickness and refractive index caused by the interaction with the particles. Interaction was measured at pH values of 3.0, 3.6, 4.4, 5.3, 6.6, and 8.0. No cleavage of the PAA chains from the surface was observed at any pH, which might be expected, for instance, by hydrolysis of the ester linkage that binds the polymer chain to the surface. It turned out that several cycles of injection were necessary to fully load the brushes with nanoparticles. In this context fully loaded means the approximation to a maximum value of response units after various cycles of injection and rinsing. The uptake of nanoparticles was investigated with a sample of 7.6 nm thickness and a molecular weight of 12 600 g/mol (DP$_n$ = 175) of the grafted PAA with nanoparticle concentrations of 10.0 and 1.0 mg/mL, Figures 11 and 12.

These results show that the interaction strongly depends on the pH. The incorporation of nanoparticles into the PAA brush is a slow and time-consuming step, which makes it necessary to repeat the injection cycles several times to approximately reach a saturation of the polymer layer. This saturation can be seen by approximation to a maximum value of ΔRU. At that point the amount of bound particles on and/or within the brush is governed by thermodynamics rather than kinetics. The initial uptake of nanoparticles is always higher in the case of the more concentrated solution. After the first injection

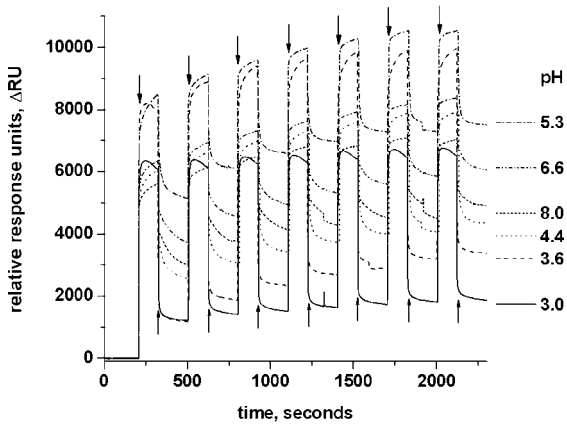

Figure 11. Nanoparticle uptake at a concentration of 10.0 mg/mL on a 7.6 nm PAA substrate. A constant uptake of particles can be seen for each injection and washing step, approaching a maximum value for each pH. Downward pointing arrows indicate the start of the injection, upward pointing arrows the end.

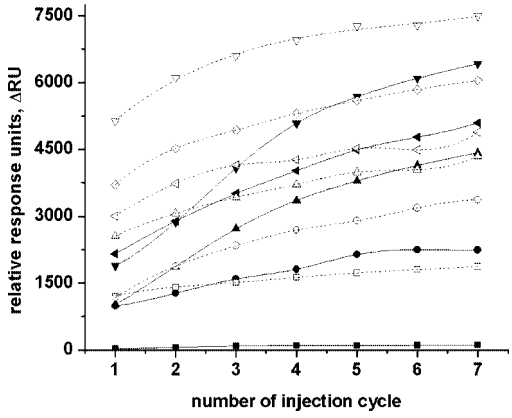

Figure 12. Increase in relative response units after each cycle of injection and washing for nanoparticle concentrations of 10.0 mg/mL (open symbols) and 1.0 mg/mL (filled symbols). Measurements were conducted at pH values of 3.0 (□), 3.6 (○), 4.4 (△), 5.3 (▽), 6.6 (◇), and 8.0 (left-pointing triangle). Dashed lines are guides to the eye.

the high-concentration solutions level off more rapidly than the low-concentration solutions; good examples for this can be seen at pH 4.4, 5.3, and 8.0 in Figure 12. After seven cycles almost the same amount of nanoparticles was adsorbed for both concentrations and is therefore concentration-independent. This point was taken to determine the optimum pH conditions for the brush−nanoparticle interaction. It can be easily seen that the interaction is strongest at about pH 5.3. Lower pH values lead to significantly less to almost no interaction; higher pH also decreases the capacity of bound particles. A significant amount can, however, still be adsorbed to the polymer.

To see whether penetration of the nanoparticles in the dense polymer brush occurs, SPR measurements were performed on systems with varying layer thickness (Figure 13). This experiment indicates that the particles penetrate the dense brushes; however, we cannot state how deep the particles penetrate the layer. With increasing layer thickness and molecular weight of the grafted PAA, the amount of adsorbed nanoparticles also increases. For each injection the SPR gives the highest signal for the thickest layer and the lowest signal for the thinnest, indicating that penetration of the particles in the brush takes place. A possible adsorption only at the polymer/air interface should result in approximately the same increase in response units, especially

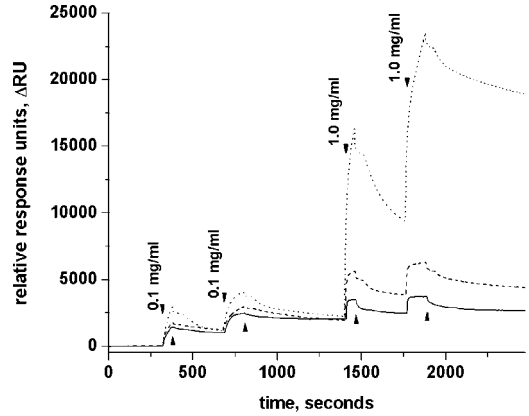

Figure 13. Uptake of nanoparticles for brushes with different layer thicknesses at pH 8.0. Solutions of 0.1 and 1.0 mg/mL nanoparticle concentration were injected as indicated (the downward pointing arrow indicates the start, upward pointing arrows the end). Layer thicknesses and corresponding molecular weights of the PAA of 7.6 nm and 12 600 g/mol (solid line), 12.7 nm and 19 300 g/mol (dashed line), and 17.2 nm and 31 100 g/mol (dotted line) were used.

since the grafting densities among the various samples are almost equal. Since the number of functional groups at the surface are not a function of the layer thickness, the same amount of particles should be adsorbed, which should reflect a similar increase in ΔRU. This behavior cannot be observed in this case.

Adsorption of the nanoparticles into the brush can also be rationalized by thermodynamic considerations. The size of the particles is small enough to almost fit into the free space around a single grafted chain, which means that the nanoparticles can mix with the brush layer and only a minor entropic penalty has to be paid for the reduction of the free volume around the PAA brushes.[34] At the same time counterion release can take place, since each nanoparticle has ca. 14 amino functions, which is entropically favorable. Finally, electrostatic attraction between the negatively charged PAA brushes and the positively charged nanoparticles (depending on the pH) can enthalpically contribute to the particle uptake and incorporation. Moreover, SANS studies recently showed that block copolymer micelles with a PAA corona strongly interact with the same nanoparticles, and these have a density located near the core of the micelle.[35]

Conclusions

Highly uniform and homogeneous brushes of PAA of various layer thicknesses were synthesized on planar gold surfaces. The binding strength of the SAM to the gold surface was of crucial importance to reproducibly hydrolyze the *tert*-butyl moieties of the grafted polymer without chain detachment. The use of methanesulfonic acid for the hydrolysis proved to be the most efficient and reproducible way. It turned out that tripod and cross-linked monolayers are suitable for that kind of hydrolysis, since they yield polymer brushes with high grafting density and are stable enough to sustain acidic hydrolysis. Polymers, which were only bound by one thiol moiety, were shown to be entirely split away. Upon hydrolysis the PtBA layers shrink by about 57%.

The pH-dependent interaction of the PAA brushes with nanoparticles was found to be highest at a pH of about 5.3. The adsorption of nanoparticles is a slow and time-consuming

(34) Kim, J. U.; O'Shaughnessy, B. *Macromolecules* **2006**, *39*, 413.
(35) Schumacher, M.; Ruppel, M.; Burkhardt, M.; Drechsler, M.; Colombani, O.; Schweins, R.; Müller, A. H. E. *Polym. Mater. Sci. Eng.* **2007**, *96*, 374.

process that has a typical time span of minutes. The nanoparticles are capable of penetrating the dense PAA layer, since the amount of adsorbed particles was found to depend on the layer thickness.

Acknowledgment. This work was supported by the Deutsche Forschungsgemeinschaft (Grant Mu896/19). We thank Dr. Joachim E. Klee (Dentsply DeTrey, Konstanz, Germany) for nanoparticle synthesis and Prof. P. Rudolf and the group of Surfaces and Thin Films (Zernike Institute for Advanced Materials) for access to the X-ray photoelectron spectrometer. Support for monolayer synthesis by Prof. W. Knoll and Dr. U. Jonas (MPI für Polymerforschung, Mainz, Germany) is appreciated. M.R. thanks the Bayerische Begabtenförderung, the Elite Network Bavaria, and the "Write it Right" workshop for ongoing support.

Supporting Information Available: Water contact angles and XPS and PM-IRRAS spectra of the monolayers not shown in the main text. This material is available free of charge via the Internet at http://pubs.acs.org.

LA8009767